Diagn Interv Radiol 2025; DOI: 10.4274/dir.2025.252878

CARDIOVASCULAR IMAGING

INVITED REVIEW

Computed tomography and magnetic resonance imaging findings in congenital cardiovascular anomalies

Mustafa Koplay
Nusret Seher

Selçuk University Faculty of Medicine, Department of Radiology, Konya, Türkiye

ABSTRACT

The incidence of congenital heart disease (CHD) is approximately 6-7 per 1,000 newborns. With advanced diagnostic, medical, and surgical methods, survival of CHD is increasing, as is the number of people living with CHD. Echocardiography is a useful modality in non-invasive imaging, whereas magnetic resonance imaging (MRI), cardiac MR (CMR), cardiac computed tomography (CT), and CT angiography (CTA) are increasingly gaining ground in congenital cardiac imaging with developing technology. Considering the limited postoperative use of echocardiography, these techniques have assumed vital roles with the increasing population of CHD in children and adults. CMR and cardiac CT can complement the information obtained with echocardiography and invasive cardiac catheterization and can sometimes provide more detail. In postoperative imaging of CHD, CMR allows an evaluation of anatomy, especially with spin echo MRI techniques, whereas cine MRI, created in gradient echo sequences, allows functional data to be obtained. Phase contrast CMR data provides information on flow direction and flow rate, allowing accurate measurement of regurgitation and shunt volume. In addition, in post-gadolinium imaging, data such as on MR angiography, myocardial perfusion, and fibrosis can be obtained with CMR. Cardiac CT and CTA provide great advantages, especially in newborns, by almost completely reducing movement and respiratory artifacts through capabilities such as high spatial and temporal resolution, fast acquisition, and short acquisition time. Three-dimensional reformatted images with contrast-enhanced CMR or cardiac CT/CTA provide excellent visualization of vascular structures in complex CHDs. Coronary imaging can be viewed more easily with CT imaging. This article reviews the literature to provide an overview of the diagnostic value, relative advantages, and overall evaluation of CMR and cardiac CT examinations in the diagnosis and postoperative follow-up of CHD.

KEYWORDS

Cardiac imaging, congenital heart disease, cardiac computed tomography, cardiac magnetic resonance imaging, computed tomography angiography, magnetic resonance angiography

Congenital cardiac malformations occur in 6-7 out of every 1,000 live births.[1] Major advances in the diagnosis and treatment of congenital heart disease (CHD) in recent years have led to increased survival rates, even in patients with the most complex malformations. Studies conducted in light of these developments indicate that the number of adults living with CHD has surpassed the number of children with CHD.[2] Echocardiography and cardiac angiography are the primary traditional imaging techniques used to evaluate patients with CHD.[3] However, these techniques have certain limitations. Echocardiography is limited by its narrow field of view, the need for an adequate acoustic window for imaging, and operator experience. Catheter angiography is limited by the superimposition of structures being examined, the risk of complications associated with the catheter, and its suboptimal evaluation of extracardiac structures. Studies have demonstrated that cardiac catheterization, the gold standard for cardiac imaging in terms of hemodynamic assessment, causes death in 1% of newborns with complex CHD.[4] In recent years, the use of cardiac computed tomography (CT) and magnetic resonance imaging (MRI) in the evaluation of this condition has increased substantially. Considering the long acquisition times of MRI and the age group of patients, MRI may require sedation and can lead to artifacts and potential anesthesia-related

Corresponding author: Mustafa Koplay

E-mail: koplaymustafa@hotmail.com

Received 09 July 2025; revision requested 28 July 2025; last revision received 08 September 2025; accepted 05 October 2025.

Epub: 17.11.2025

Publication date:

DOI: 10.4274/dir.2025.252878

You may cite this article as: Koplay M, Seher N. Computed tomography and magnetic resonance imaging findings in congenital cardiovascular anomalies. *Diagn Interv Radiol.* 17 November 2025 DOI: 10.4274/dir.2025.252878 [Epub Ahead of Print].

complications. However, recent studies have reported that the data obtained from compressed sensing four-dimensional (4D) flow MRI shows no significant difference compared with the reference standard two-dimensional (2D) phase contrast.[5] CT scans can be performed in seconds, thereby limiting the need for sedation in patients who are clinically incompatible. With isovolumetric imaging in CT, high-quality multiplanar reconstructions (MPR) and three-dimensional (3D) images can now be created. Finally, CT provides more detailed information about extracardiac structures than MRI. Imaging modalities for early and accurate diagnosis of CHD, along with advancements in surgical and medical treatments, have led to improved long-term survival.[6] To ensure that this multidisciplinary approach is properly implemented, it is essential that radiology, cardiology, and cardiovascular surgery units use a common language in classifying and defining these diseases so that they can play a role in the diagnosis and follow-up of CHD. In this review, CT and MRI findings in CHD are discussed.

Computed tomography in congenital heart disease

Multi-detector CT (MDCT) scanners quickly collect volumetric data with high spatial resolution. The increased scanning speed reduces motion and breathing artifacts during imaging, enabling images to be obtained at high heart rates.[7] By completing the scan in a very short time, it also eliminates the need for sedation.[8] Although recent advancements in scanners and protocols have reduced radiation exposure, radiation remains a key concern for children. In addition to cardiac anatomy, CT angiography (CTA) with CT imaging helps evaluate the lung parenchyma, chest wall structures, tracheobronchial structures, and related pathologies of the aorta–pulmonary vascular structure.[9] Data from CT is analyzed in three orthogonal planes (axial, coronal, and sagittal) using MPR. The volume rendering technique allows for 3D visualization of cardiac and extracardiac morphology. Cardiac CTA (cCTA) is a highly successful imaging modality in pediatric cardiac imaging; however, it has poorer temporal resolution than other cardiac imaging techniques, such as echocardiography, cardiac catheterization, and cardiac MR (CMR).[10] In the literature, a 64-slice MDCT system is considered the minimum adequate modality for the evaluation of coronary heart disease and coronary artery disease, as well as for optimizing image quality through radiation dose-reduction and noise-reduction algorithms.[11] In pediatric populations, however, given the higher likelihood of heart rate and respiratory artifacts, faster scanners equipped with wider detector coverage are recommended.[12] Advances in MDCT technology, including faster and broader collimation as well as higher gantry rotation speeds, have led to reduced scan times, enhanced temporal resolution, and, as a result, diminished motion and respiratory artifacts.[13] Functional assessment is generally feasible with MDCT scanners with 256 slices or more. Next-generation MDCT scanners, including 256–320/640-slice systems and dual-source MDCT, achieve a 50%–70% reduction in radiation exposure through shorter scan times, reaching as low as 0.12 seconds.[13,14] Functional cardiac assessment is generally feasible with scanners of 256 slices or more.[15] Moreover, recent studies in pediatric cardiac imaging indicate that photon-counting CT offers superior resolution and a reduced radiation dose when compared with dual-source CT.[16] Contrast medium (CM) is required for all scans, and the CM dose is determined based on body weight. For imaging without coronary arteries, the routine dose is 1.0 mL/kg of CM containing 300 mg of iodine per mL, and for imaging with coronary arteries, the dose is 1.0–1.2 mL/kg of CM containing 350–370 mg of iodine per mL.[17]

Main points

- The use of cardiac computed tomography (CT) and magnetic resonance imaging (MRI) in the diagnosis and postoperative follow-up of congenital heart disease (CHD) is steadily increasing.
- Cardiac CT, with its high spatial and temporal resolution, rapid acquisition, and reduced motion artifacts, plays a crucial role, particularly in newborns and in the evaluation of complex vascular anomalies.
- Cardiac MRI, as a radiation-free modality, is advantageous for long-term follow-up and provides valuable functional information, including ventricular performance, flow quantification, shunt assessment, and myocardial fibrosis detection.
- Both modalities complement the limitations of echocardiography and invasive angiography, offering critical data for surgical planning and postoperative management.
- Ongoing technological advances have enabled lower radiation doses, shorter imaging times, and improved image quality, thereby contributing to the prognosis and long-term outcomes of pediatric and adult patients with CHD.

Cardiac computed tomography angiography and computed tomography angiography techniques

There are primarily two imaging techniques: non-electrocardiogram (ECG)-triggered and ECG-triggered imaging. Non-ECG-triggered CTA is primarily used for evaluating non-cardiac structures, whereas ECG-triggered imaging is primarily used for coronary artery imaging.[15] ECG-triggered imaging has two modes: prospective and retrospective ECG-triggered imaging.[14] Retrospective ECG-triggered imaging acquires data for the R–R interval of a complete cardiac cycle, thereby enabling multisegmental reconstruction, improved temporal resolution, and assessment of left ventricular function. However, despite these advantages, it results in 3–5 times the radiation exposure of prospective imaging.[13] Additionally, it allows imaging at heart rates of up to 170 bpm. In prospective ECG-triggered imaging, high pitch values and dual-source devices enable imaging. This technique can also be referred to as the "step and shoot" technique. It is necessary for the heart rate to remain low, and more importantly, stable.[18,19] In this technique, the CT scanner is positioned during the R–R cycle of the heart, applying maximum tube current only at end diastole in adults and early systole in children and completely stopping radiation during the remainder of the cardiac cycle, thereby reducing the dose.[20] The use of a low tube current and the inability to visualize all phases of the heart limit functional assessment.[18] Table 1 presents the technical specifications and protocols of next-generation CT systems.[16]

Cardiac magnetic resonance imaging in congenital heart disease

In recent years, CMR has gained importance in the evaluation of complex malformations and the morphological and functional assessment of CHDs.[21] Due to the absence of ionizing radiation, it is ideal for long-term CHD follow-up. Moreover, it provides blood flow data, and detailed functional assessment can be performed using cine images.[18] CMR provides images that can serve as standard references for the accurate and reproducible quantification of right and left ventricular volumes, mass, and function.[22] The steady-state free precession (SSFP) sequence is preferred in CMR examinations because it provides good contrast between blood and the myocardium. The 2D "white blood" SSFP sequence can provide dynamic information about the heart and large vessels.[23] The "black blood" spin echo sequences

Table 1. Technical characteristics of new-generation computed tomography scanners and recommended parameters for contrast media injection

	DSCT (2 × 192)	PCCT (2 × 144)
Extracardiac structure	Non-ECG gated	Non-ECG gated
Intracardiac structure/coronary arteries	ECG gated	ECG gated
Spatial resolution (mm)	0.24	0.11
Temporal resolution (msec)	66	66
Gantry rotation time (sec)	0.25	0.25
Maximum scan speed (mm/sec)	737	737
Tube voltage (kVp)	70	90
Tube current (mA)	Automatic modulation	Automatic modulation
Pitch	3.0	3.0
Iterative reconstruction	Available	Available
Mean dose (mSv)	0.50	0.52
Contrast medium	Iodine	Iodine
Concentration	320–370 mg/mL	320–370 mg/mL
Dose	1–1.2 mL/kg	1–1.2 mL/kg
Injection rate	1.5–4 mL/second	1.5–4 mL/second

DSCT, dual-source computed tomography; PCCT, photon-counting computed tomography; kVp, kilovoltage peak; mA: milliampere; mSv, milisievert; ECG, electrocardiogram.

obtained with the double inversion recovery technique provide static high-resolution images. Another advantage is the minimal presence of metallic artifacts in these sequences. Images obtained with the 3D isotropic SSFP sequence allow evaluation in different planes without loss of resolution.[24] CMR is the preferred technique for assessing valvular insufficiency, with shunt quantification based on pulmonary-to-systemic flow ratios (Qp/Qs) achievable through flow measurements in the main pulmonary artery and aorta.[25] Additional advantages of CMR include comprehensive evaluation and grading of valvular dysfunction, accurate shunt quantification, detailed flow assessment, and non-invasive tissue characterization.[26] Recent studies have demonstrated that advancements in 4D phase contrast velocity mapping yield novel insights into cardiovascular hemodynamics, which are of particular relevance for surgical reconstruction. This is especially crucial in patients with single-ventricle physiology undergoing cavopulmonary connection. Furthermore, 4D flow MRI has been established as the non-invasive gold standard for postoperative follow-up of procedures such as the Fontan operation.[27] For contrast-enhanced MR angiography (MRA), a breath-hold 3D spoiled gradient echo sequence without ECG triggering is preferred.[28] It is particularly useful in evaluating abnormal pulmonary or systemic venous return and aortic coarctation (CoA), as well as in postoperative follow-up, and it correlates well with conventional angiography and CTA in identifying stenotic vascular structures.[29] In cases where contrast is contraindicated, the 3D SSFP sequence can be used. In delayed contrast studies, it enables the assessment of myocardial scarring and fibrosis, providing prognostic information for patients with ventricular dysfunction or myocardial evaluation following surgical repair.[30] Table 2 outlines the clinical scenarios in which specific CMR sequences should be applied.[31] Recent studies have highlighted the value of T1, T2, and extracellular volume mapping and dark- or gray-blood late gadolinium enhancement techniques for tissue characterization and the detection of subendocardial scarring in CHD.[32] Although CMR has become safer, it remains challenging in patients with metallic implants and pacemakers. Therefore, all cardiac imaging modalities are complementary, and it is essential to understand their strengths and weaknesses to optimize the use of various imaging modalities (Table 3).[2]

Acyanotic heart defects: conditions and imaging considerations

Atrial septal defect

Atrial septal defects (ASDs) are the most common congenital heart defects detected in adults (Figure 1).[33] There are three main types: secundum ASDs account for 75%, primum ASDs for 20%, and sinus venosus ASDs for 5%.[34] Coronary sinus-type ASDs are the rarest. cCTA and CMR are useful for detecting associated abnormal pulmonary veins located above the level of the azygos vein in the superior vena cava. The presence of an ASD causes left-to-right shunting, leading to atrial and ventricular enlargement on the right side. ASDs are also an independent risk factor for thromboembolic stroke.

Ventricular septal defect

Ventricular septal defects (VSDs) are a shunt that occurs between the right ventricles (RVs) and left ventricles (LVs) through a defect in the ventricular septum (Figure 2). VSDs are the most common type of CHD detected in newborns,[35] and they can occur in isolation or with other anomalies. When associated with multiple anomalies, if the most notable hemodynamic abnormality is the shunt associated with the VSD, the VSD is considered the primary anomaly.[36] VSD classifications are based on the location of the defect, and the most common type is the perimembranous type. Other types include the muscular, outlet, and inlet types. Both MRI and CT are useful in determining the location and type of a VSD.[37]

Atrioventricular septal defect

Atrioventricular septal defects (AVSDs) are also known as endocardial cushion defects or atrioventricular canal defects (Figure 3). These types of defects involve the atrial and ventricular septum, with one or both of the mitral and tricuspid valves.[38] Clinical findings may present as complete defects (ASDs and VSDs) or partial defects (only ASDs).[39] AVSDs result from the underdevelopment of the apical portion of the atrial septum, the basal portion of the ventricular septum, and the AV valves. In this defect, the four chambers of the heart are generally interconnected, allowing shunts to form from left to right or right to left. There is a strong association between AV canal defects and trisomy 21, with a risk of trisomy 21 being as much as 50% in fetuses with AV canal defects.[40] Classification is based on complete and partial types. In the complete type, a posterior or inlet VSD is accompanied by a primum ASD and a common AV valve. In the partial type, a VSD is not present, and there is a single AV valve annulus with two separate valve orifices.[41] The most common partial form involves primum ASDs and a cleft in the anterior leaflet of the mitral valve.[38]

Patent ductus arteriosus

The ductus arteriosus (DA), a normal vascular structure connecting the pulmonary artery and the aorta during fetal life, allows blood from the RV to pass into the aorta. The DA accounts for 41% of total cardiac output.[42]

Table 2. Indications for the use of specific sequences in cardiac magnetic resonance imaging

Sequence	Indication
Cine bSSFP	RV/LV size, shape, and volume; atrial size and shape; ventricular function; mass and EF; LVOT/RVOT obstruction; assessment of pulmonary artery anatomy and pulsatility; aortic valve morphology; aortic anatomy; measurement of aortic root; ascending aorta and aortic arch
Tagging	Screen for fusion of pericardium and myocardium in constriction
Phase contrast flow	Pulmonary regurgitation, differential pulmonary blood flow, aortopulmonary collateral flow measurement, Qp/Qs measurement in the context of a suspected shunt, valve dysfunction
Black blood imaging (especially with metallic artifacts)	Arterial or venous evaluation
Contrast-enhanced magnetic resonance angiography	Indicated as part of first study: pulmonary artery and vein anatomy, extracardiac vascular anatomy
T1- or T2-weighted with post-gadolinium spin echo or cine SSFP	Pericardial layer or fluid characterization
3D bSSFP imaging	Intracardiac anatomy
4D flow imaging	Assessment of pulmonary arterial pressures, wall shear stress, RV diastolic function
T2 imaging and/or mapping	Myocardial edema
T1 mapping (native)	Myocardial characterization
T1 mapping (post contrast)	Myocardial characterization, extracellular volume
Early gadolinium enhancement	Hyperemia
Late gadolinium enhancement	Myocardial inflammation, fibrosis, fat

3D, three-dimensional; 4D, four-dimensional; EF, ejection fraction; LV, left ventricular; RV, right ventricular; bSSFP, balanced steady-state free precession; LVOT, left ventricular outflow tract; RVOT, right ventricular outflow tract; Qp/Qs, pulmonary–systemic flow ratio.

Table 3. Relative advantages of CMR and CT/CTA

	CMR	CT/CTA
Morphology	++++	++
Function	++++	++ (with ECG gated)
Extracardiac structure	++	++++
Ventricular volumes	++++	++
Flow quantification	++++	–
Myocardial perfusion	++++	++
Myocardial viability	++++	++
Intracardiac anatomy	++++	++
Coronary artery evaluation	+	++++
Radiation	–	++++
Examination time	++++	+
Contrast allergy	+	++
Emergency case	++	++++
Real-time viewing	++++	–
Calcium imaging	+	++++
Long-axis resolution	+	++++
Trained radiologists	+	++

CMR, cardiac magnetic resonance; CT, computed tomography; CTA, computed tomography angiography; ECG, electrocardiogram.

Unlike other vascular structures, the media layer of the DA contains smooth muscle.[43] After birth, this smooth muscle contracts and thickens, thereby reducing the lumen size and causing the functional closure of the DA. Functional closure occurs in 44% of infants within 24 hours and in 88% within 48 hours. Failure of the DA to close postnatally results in patent DA (PDA) (Figure 4). The incidence of PDA in term infants ranges from 3 to 8 per 10,000 live births and is more common in female infants.[44] Prematurity is the most important risk factor for PDA, and the risk of PDA in premature infants is generally more than 10 times higher.[45] Although both right and left PDA are possible, the most common type is left-sided PDA between the main pulmonary artery and the proximal descending aorta.[46] PDAs are classified into five types based on their angiographic appearance, as described by Krichenko et al.[47] The hemodynamic outcomes of PDA vary depending on the extent of the left-to-right shunt. In a small PDA, the pulmonary–systemic flow ratio (Qp/Qs) is <1.5, in a medium-sized PDA, it is <2.2, and in a large PDA, it is >2.2.[48]

Partial anomalous pulmonary venous drainage

A defect in the normal embryonic development of the pulmonary veins can lead to congenital anomalies ranging from partial anomalous pulmonary venous connection (PAPVC) to total anomalous pulmonary venous connection. Abnormal pulmonary venous variations can be seen in up to 38% of the population.[49] The most common type is drainage of the right pulmonary vein into the superior vena cava or right atrium (Figure 5).[50] The anomaly may be associated with the presence of an associated ASD or may occur as part of a complex CHD. Associated congenital anomalies serve as the main determinants of morbidity and mortality in PAPVC.[51] Currently, MDCT and MRA have replaced traditional imaging techniques and provide optimal evaluation capabilities.

Aortic stenosis

Left ventricular outflow tract obstructions account for 6% of CHD cases (Figure 6),[26]

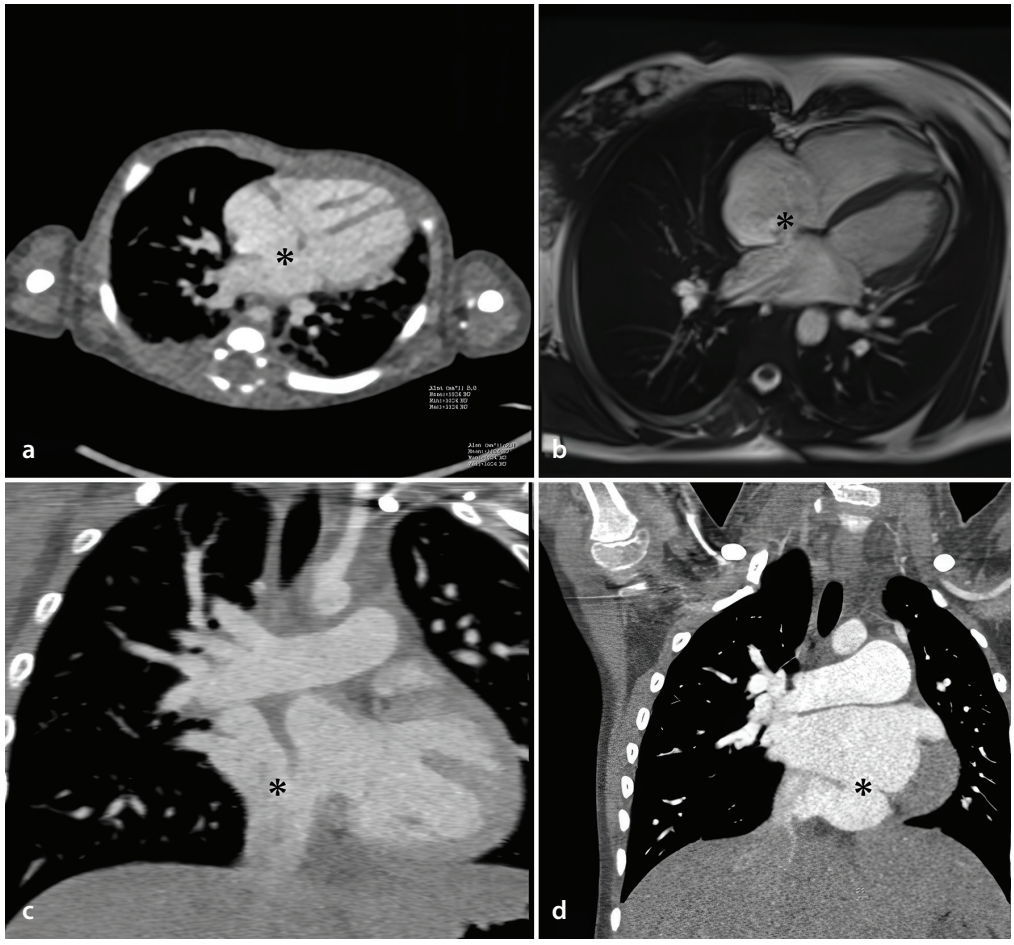

Figure 1. Primum-type atrial septal defect (ASD; black star) in an axial computed tomography angiography (CTA) image **(a)**, secundum-type ASD (black star) in a four-chamber cine cardiac magnetic resonance image **(b)**, sinus venosus-type ASD (black star) in a coronal CTA image **(c)**, and coronary sinus-type ASD (black star) in a coronal CTA image **(d)**.

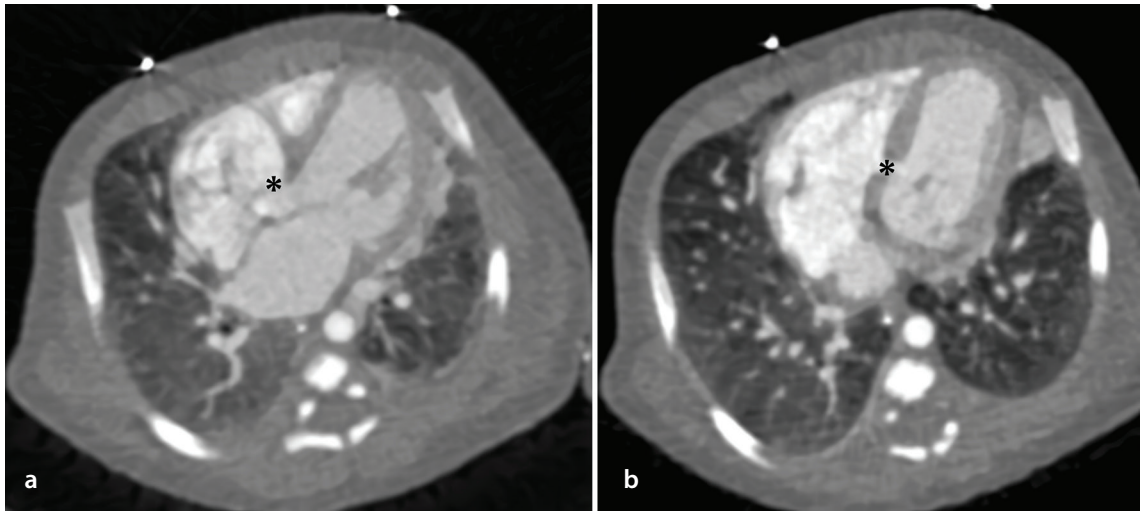

Figure 2. Axial computed tomography angiography images: **(a)** perimembranous-type (black star) and **(b)** muscular-type ventricular septal defects.

with valvular aortic stenosis (AS) accounting for 70%.[52] Valvular AS most commonly occurs secondary to a bicuspid aortic valve, and it may be accompanied by Turner syndrome. Critical neonatal AS is characterized by a myxomatous valve and an aortic valve opening as small as a needle tip. The aortic valve is typically hypoplastic, and mitral valve hypoplasia, left ventricular hypoplasia, and VSDs frequently accompany it.[40] Supravalvular AS is rarely seen, and Williams syndrome is present in 30%–50% of cases. The subvalvular type accounts for 10%–20% of cases. It causes narrowing due to a simple membrane or a fibromuscular structure resembling a long tunnel in the left ventricular outflow tract. It is often associated with other left ventricular anomalies, including Shone complex.[40]

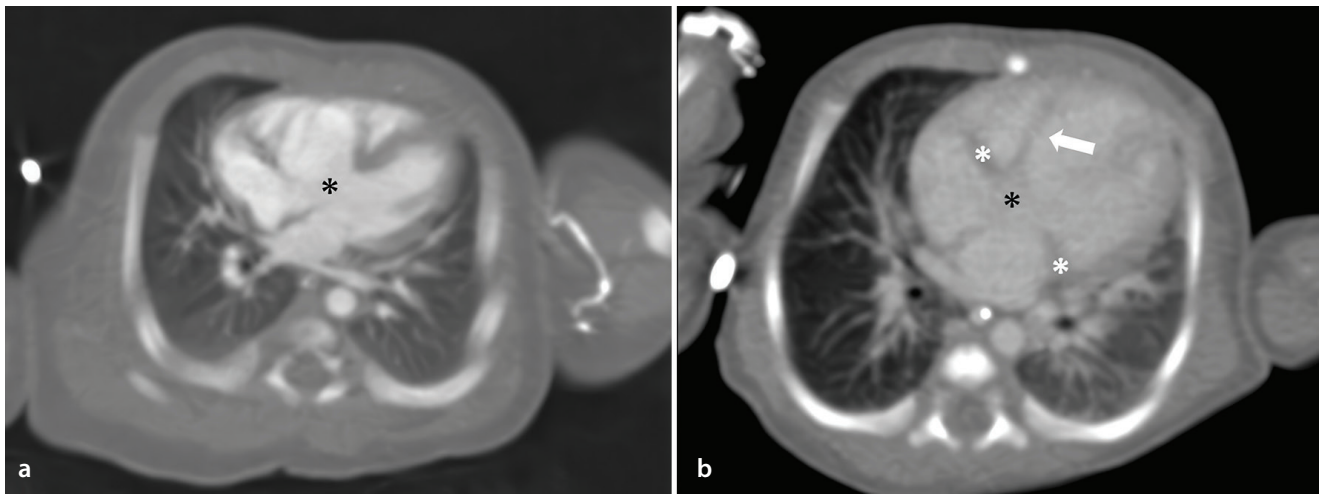

Figure 3. Axial computed tomography angiography images: complete-type **(a)** atrioventricular septal defect (AVSD; black star) [primum-type atrial septal defect (ASD)], membranous-type ventricular septal defect, single AV valve) and incomplete-type **(b)** AVSD (black star) [primum-type ASD and two separate valves (white stars)]. The interventricular septum (white arrow) is intact.

Figure 4. Type A patent ductus arteriosus (PDA; black arrow) in a three-dimensional (3D) volume rendered image **(a)**, Type B PDA (black arrow) in a sagittal reformatted computed tomography angiography image **(b)**, and Type E PDA (black arrow) in a 3D volume rendered image **(c)**.

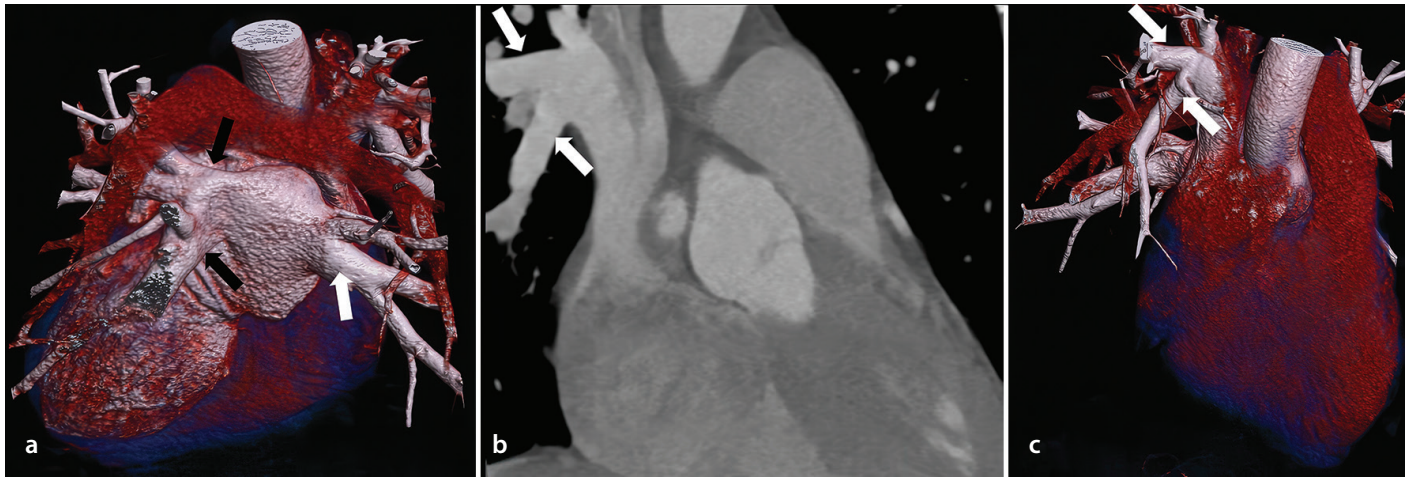

Figure 5. In the three-dimensional (3D) volume rendered cardiac computed tomography (CT) **(a)** image of a 25-year-old male patient, the left pulmonary veins (black arrows) and the right inferior pulmonary vein (white arrow) open into the left atrium, whereas in the coronal cardiac CT **(b)** and 3D volume rendered **(c)** images, the right upper pulmonary vein, formed by the union of two veins, opens into the superior vena cava (white arrows).

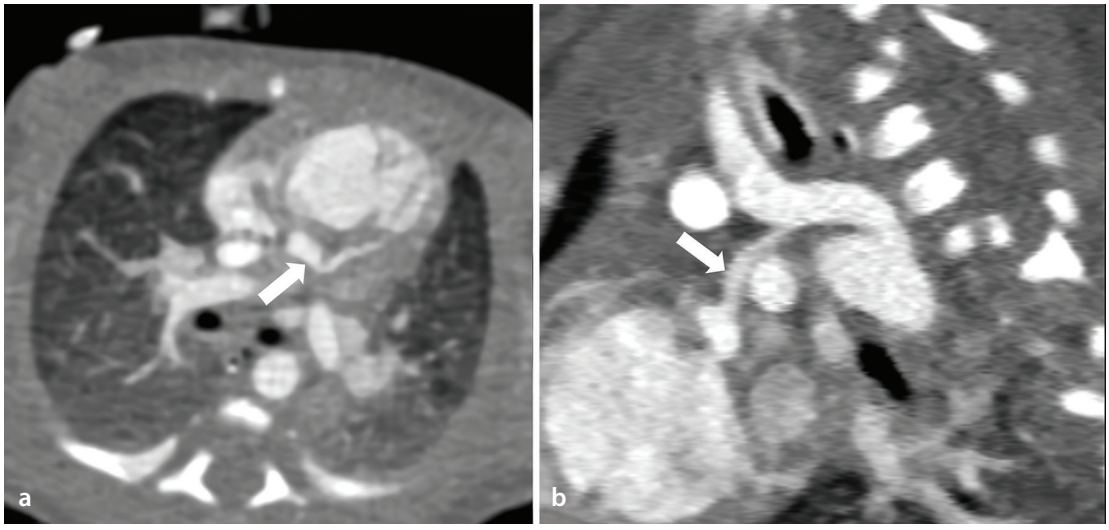

Figure 6. Axial **(a)** and sagittal reformatted **(b)** computed tomography angiography images of a 6-day-old female patient showing supravalvular diffuse aortic stenosis (white arrows).

Pulmonary stenosis

Pulmonary stenosis (PS) accounts for 8%–12% of CHDs,[40] with valvular PS the most common type (Figure 7). The pulmonary valve has thickened leaflets, and the commissures may be absent or fused. In most patients, the pulmonary valve appears dome shaped. Severe PS is associated with right ventricular and infundibular muscle hypertrophy.[39] Critical PS is the most serious type of PS, resulting in inadequate pulmonary blood flow, and is seen in 10%–20% of patients. Dysplastic pulmonary valve is associated with Noonan syndrome.[53] Tricuspid atresia, tetralogy of Fallot (ToF), and transposition of the great arteries (TGA) may accompany PS. Alagille, Williams, and congenital rubella syndromes are associated with peripheral-type PS.[54]

Aortic coarctation

CoA accounts for 5%–8% of CHDs (Figure 8),[55] and may occur in isolation or in association with other cardiovascular anomalies, such as bicuspid aortic valve (50%–75%), aortic arch hypoplasia, subaortic stenosis, mitral valve abnormalities, AVSDs, and PDAs.[56] CoA is generally sporadic and may be accompanied by extracardiac anomalies. Cerebral aneurysms are observed in 2.5%–10% of patients with CoA.[57] Preductal CoA occurs proximal to the DA and is typically seen in newborns.[58] Moreover, preductal CoA is the most common type of coarctation in Turner syndrome.[59] Postductal coarctation, however, typically occurs after the neonatal period and is anatomically located distal to the insertion of the DA. Patients with postductal coarctation are generally asymptomatic and are diagnosed based on decreased femoral artery pressure and systemic arterial hypertension.[56]

Interrupted aortic arch

Interrupted aortic arch is a rare congenital anomaly, with an incidence of approximately 2 in 100,000.[60] It is characterized by the complete absence of connection between the ascending and descending aorta and may be connected by a remnant fibrous band. Blood flow to the descending aorta is usually via a

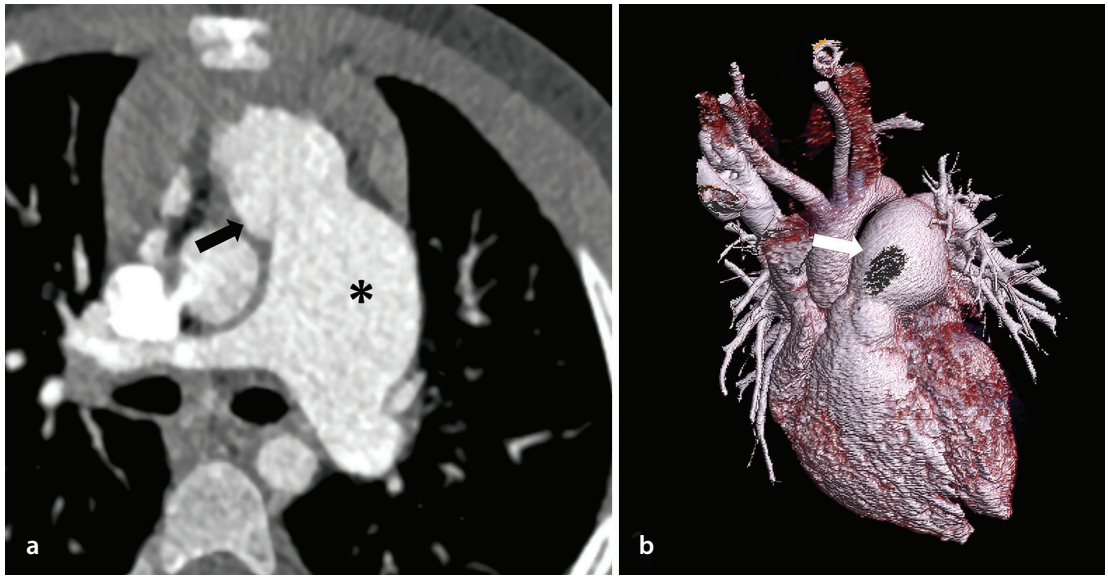

Figure 7. In the axial cardiac computed tomography angiography image **(a)** of a 6-year-old girl, stenosis (black arrow) and poststenotic dilatation (star) at the pulmonary valve level are observed. In the three-dimensional volume rendered image **(b)**, poststenotic dilatation is seen more clearly (white arrow).

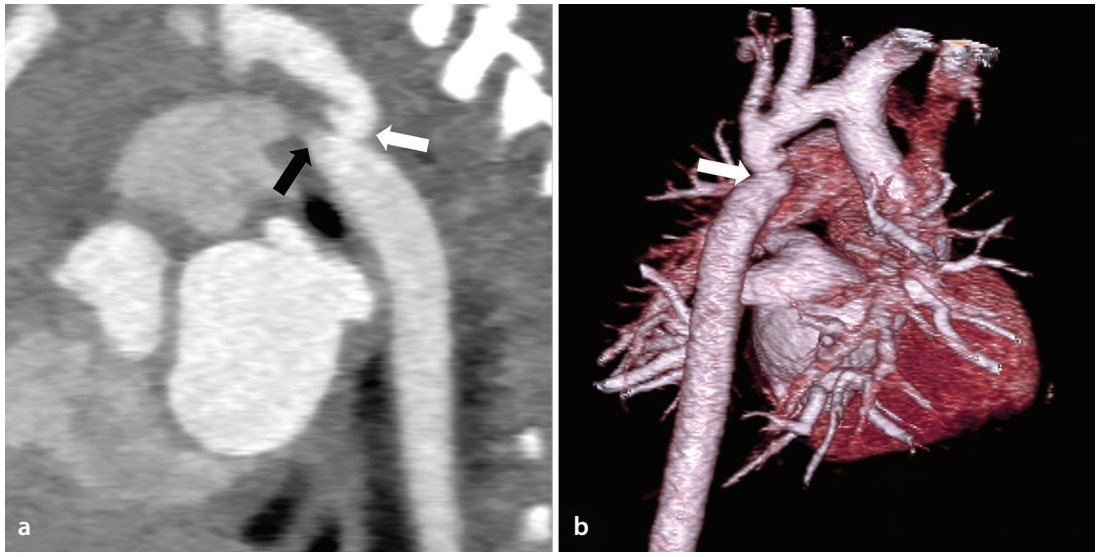

Figure 8. A 10-day-old male patient: sagittal computed tomography angiography image **(a)** showing a coarcted segment (white arrow) and patent ductus arteriosus at the level of the aortic isthmus (black arrow). In the three-dimensional volume rendered image **(b)**, the coarcted segment can be clearly seen (white arrow).

PDA. Interrupted aortic arch clinically resembles CoA, but the underlying mechanisms are thought to be different.[61] Interrupted aortic arch is classified into three types (A, B, and C) based on the location of the aortic interruption relative to the arch vessels. Type A occurs when the interruption is distal to the left subclavian artery (Figure 9), type B when it is between the carotid and subclavian arteries, and type C when it is between the carotid arteries. Subtypes are classified based on the normal or abnormal origin of the right subclavian artery. In the normal origin of the right subclavian artery (subtype 1), the aberrant right subclavian artery originates distally from the left subclavian artery (subtype 2), and the isolated right subclavian artery originates from the right DA (subtype 3).[62] Interrupted aortic arch is typically associated with a large VSD or PDA or, less commonly, with an aortopulmonary window or truncus arteriosus (TA).[61]

Cyanotic heart defects: conditions and imaging considerations

ToF is the most common cyanotic CHD, occurring in approximately 1 in 3,600 live births.[63] There are four anatomical features: a VSD, an overriding aorta, a pulmonary outflow tract obstruction, and right ventricular hypertrophy (Figure 10).[64] Anterior deviation of the conal septum and infundibular hypoplasia cause pulmonary outlet obstruction. The primary problem in ToF is the inadequate development of the pulmonary infundibulum,[64] and the pulmonary valve is often abnormal. In patients with atresia, pulmonary blood flow is maintained via a PDA. The VSD is typically located in the membranous septum. In the variant of ToF with absent pulmonary valve, RV and pulmonary arterial dilatation are observed. When ToF is accompanied by an ASD, it is named Fallot's pentalogy. The degree of pulmonary regurgitation plays a key role in ToF follow-up (Figure 11).[65] In particular, quantification of RV volumes and function using CMR is indispensable for treatment protocols.[66]

Transposition of the great arteries

TGAs refers to a condition in which the aorta originates from the RV and the main

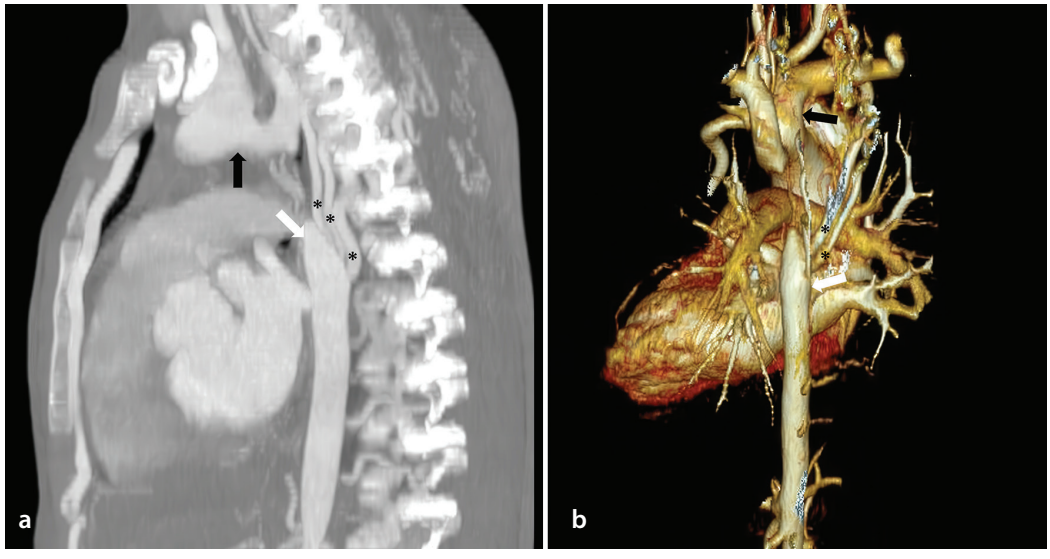

Figure 9. A 19-year-old male patient diagnosed with interrupted aortic arch (Type A): the aortic arch is normal (black arrows) in the sagittal reformatted computed tomography angiography image **(a)** and three-dimensional volume rendered image **(b)**, but an interruption is observed between the descending aorta (white arrows) and the left subclavian artery distal to it. Numerous collateral vascular structures draining into the descending aorta are observed (black stars).

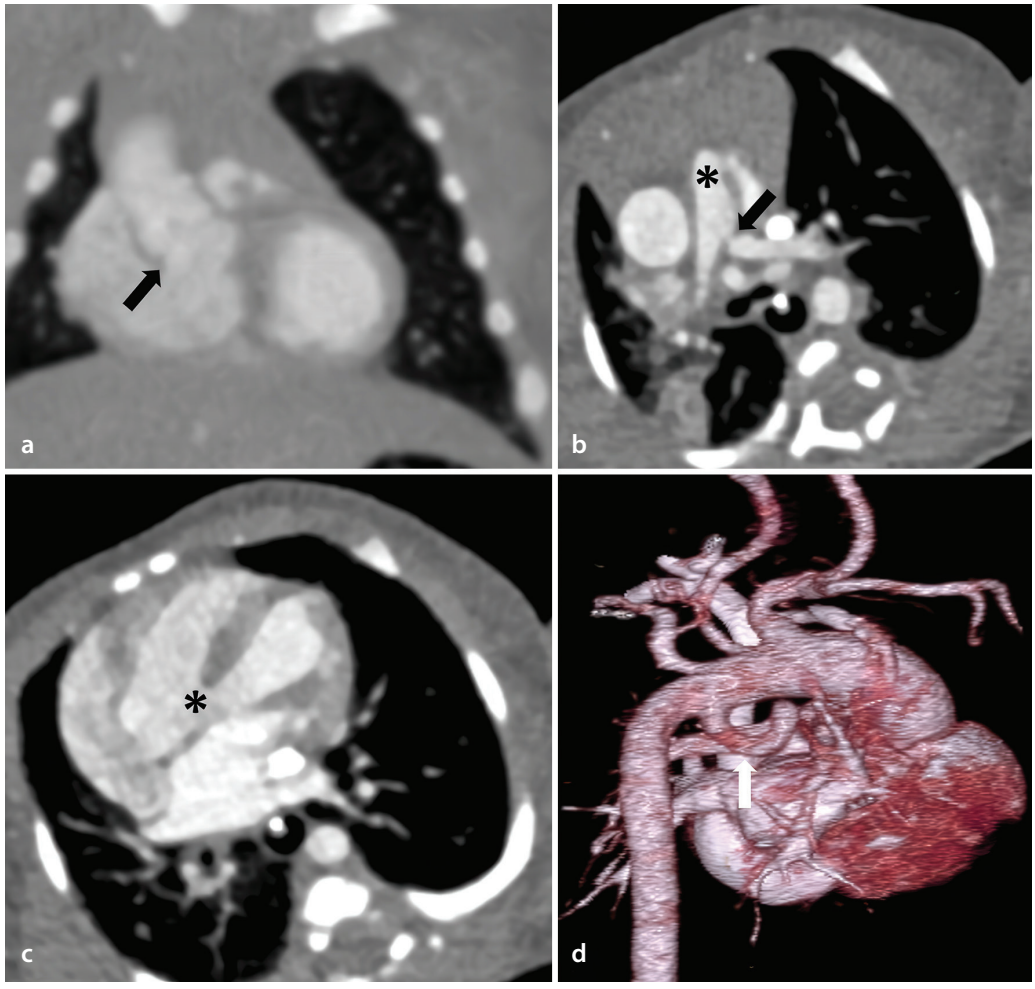

Figure 10. Male patient diagnosed with 2-day-old tetralogy of Fallot: dextroposed aorta is observed in a coronal computed tomography angiography (CTA) image **(a)** (black arrow), pulmonary trunk hypoplasia (star) and notable stenosis in the left pulmonary artery root (black arrow) in an axial CTA image **(b)**, perimembranous ventricular septal defect (black star) in an axial CTA image **(c)**, and patent ductus arteriosus in a three-dimensional volume rendered image **(d)** (white arrow).

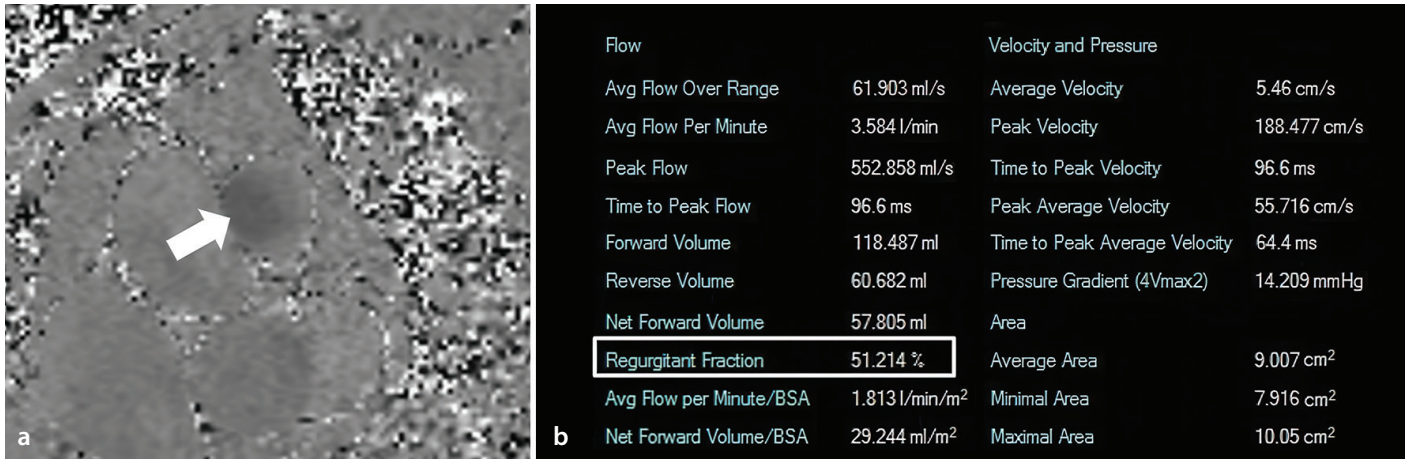

Figure 11. Control cardiac magnetic resonance image of a 62-year-old male patient who underwent surgery for tetralogy of Fallot 40 years ago: phase contrast flow examination **(a)** showing notable insufficiency findings in the pulmonary valve. Calculations made from the pulmonary valve **(b)** show a 51% regurgitation fraction in the pulmonary valve.

pulmonary artery originates from the LV (ventriculoarterial discordance).[67] The most common form is known as complete transposition and is often referred to as dextro-TGA or d-loop TGA (Figure 12). Complete transposition is characterized by AV concordance (the LV is connected to the left atrium and the pulmonary artery, whereas the RV is connected to the right atrium and the aorta). Congenital corrected TGA, also known as l-loop or L-TGA, is characterized by AV discordance (the left atrium is morphologically connected to the RV, and the right atrium is morphologically connected to the LV).[68] The incidence of TGA is 1 in 2,000 to 5,000 live births.[63,69] TGAs

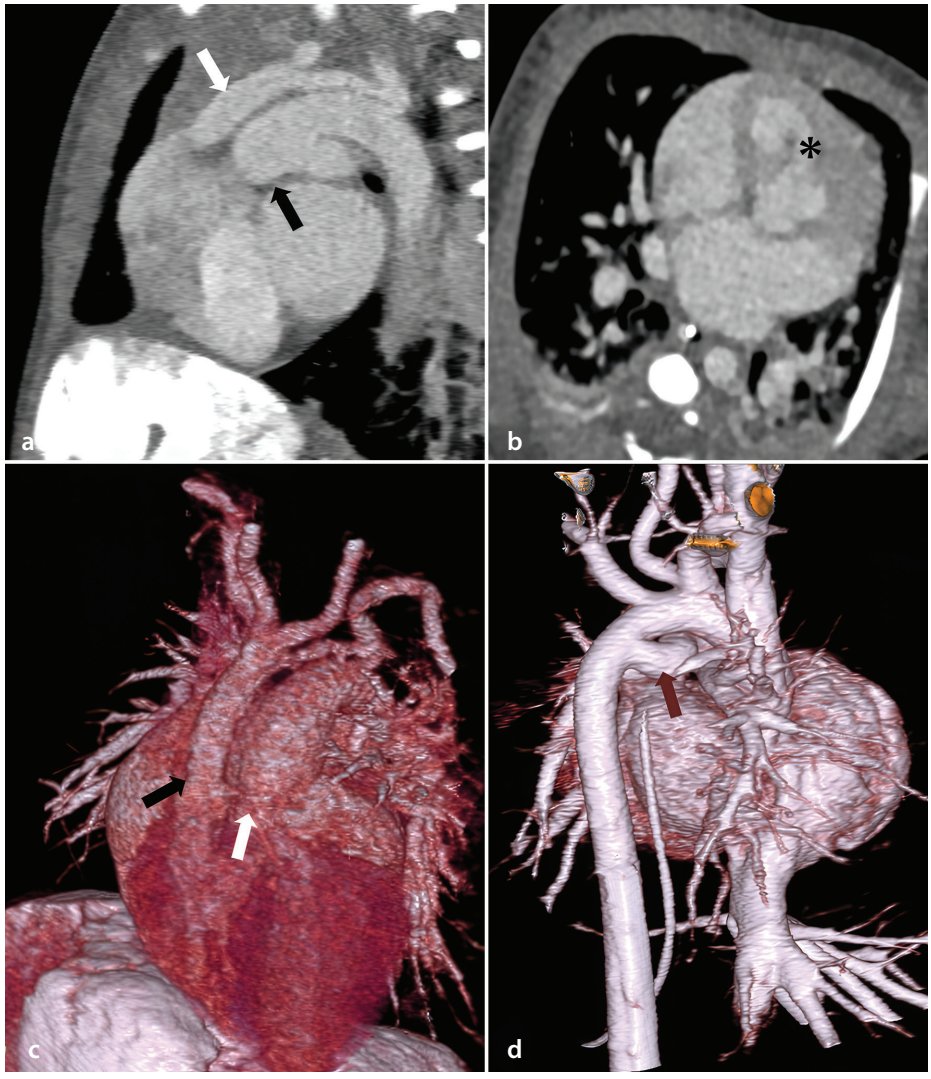

Figure 12. Patient diagnosed with 1-day transposition of the great arteries: sagittal computed tomography angiography (CTA) image **(a)** showing the aorta originating from the right ventricle and anteriorly (white arrow) and the pulmonary artery originating from the left ventricle and posteriorly (black arrow); axial CTA image **(b)** showing a membranous-type ventricular septal defect (black star). In three-dimensional volume rendered images **(c, d)**, the aorta originates from the right ventricle and anteriorly (black arrow), the pulmonary trunk originates from the left ventricle and posteriorly (white arrow), and there is a distinct patent ductus arteriosus (red arrow) between the aorta and pulmonary artery.

accounts for 5% to 7% of CHDs and 10% of all neonatal cyanotic CHDs.[70] A VSD is the most common associated anomaly (50%), and an ASD and PDA may also be present. It is the cyanotic CHD that presents with the earliest findings in newborns. Thoracic CTA is a highly useful imaging modality for diagnosis, as it can be performed rapidly and provides evaluation of vascular structures and surrounding tissues. Moreover, CMR can be used preoperatively to measure LV mass, function, and volume and to assess associated anomalies.[67]

Truncus arteriosus

TA is a rare cyanotic CHD in which a single common trunk emerges from the heart instead of the aorta and pulmonary artery.[71] A VSD is always present, and the atria and ventricles are usually normal.[72] TA accounts for 1% to 2% of CHDs,[62] and is associated with DiGeorge syndrome. It is classified into subtypes according to the Collet and Edwards classification. In Type I (50%–70%), the pulmonary trunk arises from the common trunk and divides into the right and left pulmonary arteries (Figure 13). In Type II (30%–50%), the right and left pulmonary arteries arise separately from the posterior portion of the common trunk. In Type III (6%–10%), the pulmonary arteries arise from the lateral aspect of the common trunk.[69] In Type IV, pulmonary atresia (PA) is present and may be accompanied by VSDs, PDA, and major aortopulmonary collateral arteries (MAPCAs). In the revised classification by Van Praagh, Type IV is not considered a subtype of TA but rather a variant of PA.[64] Patients are initially asymptomatic due to high pulmonary vascular resistance but begin to develop symptoms as pulmonary vascular resistance decreases over several weeks.[72] Cyanosis is typically minimal but increases as pulmonary artery stenosis becomes more pronounced.[73] Preoperative CT or MRI is generally helpful in distinguishing the branching of the pulmonary arteries and the presence of MAPCAs, pulmonary venous drainage, aortic arch anomalies, and complex anatomy in the newborn.[74]

Double outlet right ventricle

Double outlet RV (DORV) is a CHD in which both the aorta and the pulmonary trunk originate from the RV (Figure 14),[75] and a VSD is always present. Classification is based on the relationship of the VSD to the great vessels. The type associated with subaortic VSDs (50%) is the most common. The type associated with subpulmonary VSDs is also known as the Taussing–Bing anomaly. The type associated with bilateral VSDs and the type as-

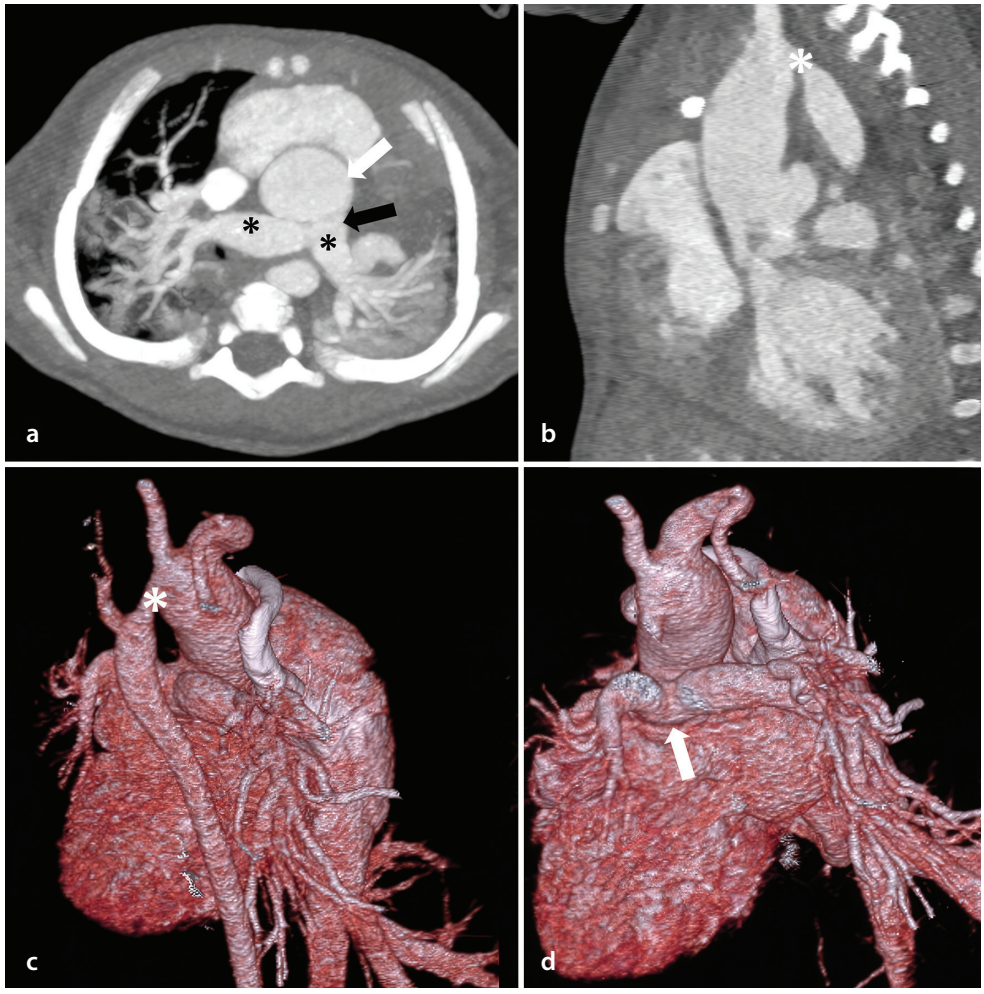

Figure 13. A 3-day-old male patient diagnosed with truncus arteriosus Type I: the common trunk (white arrow), the pulmonary trunk branching from the trunk (black arrow), and both main pulmonary arteries are seen in the axial computed tomography angiography (CTA) image **(a)** (black stars). In the sagittal CTA image **(b)** and three-dimensional (3D) volume rendering image **(c)**, the accompanying aortic coarctation is seen (white stars). In the 3D volume rendering image **(d)**, the pulmonary trunk arising from the common trunk is clearer (white arrow).

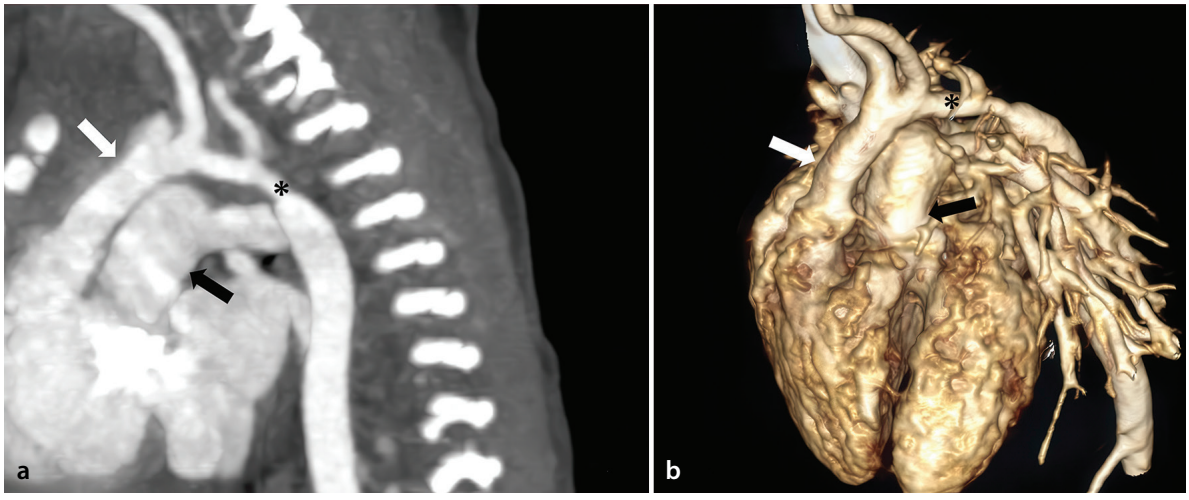

Figure 14. Female patient diagnosed with 3-day double outlet right ventricle: sagittal computed tomography angiography (CTA) **(a)** and three-dimensional volume rendered **(b)** thoracic CTA images show the aorta (white arrows) and pulmonary trunk (black arrows) originating from the right ventricle and accompanying hypoplasia (black star) in the aorta.

sociated with distally located VSDs are rare.[76] Ventricular function is important to monitor in patients with DORV, so CMR is particularly important.[77]

Tricuspid atresia

Tricuspid atresia is a CHD characterized by agenesis or congenital absence of the tricuspid valve.[73] It accounts for 1.4% of patients with CHD, is the third most common type of cyanotic CHD (Figure 15), and is the most common cause of cyanosis and left ventricular hypertrophy.[78] It is often associated with right ventricular hypoplasia and VSDs, and pulmonary blood flow is shunted via the DA. Tricuspid atresia classification is subdivided into subtypes based on PS and the position of the great arteries. In Type 1, the great arteries are normal (the most common type); in Type 2, ToF is present; and in Type 3, complex anomalies such as TA or AVSD accompany ToF or malposition.[72]

Ebstein anomaly

Ebstein anomaly (EA) is a malformation of the tricuspid valve (Figure 16). The septal and posterior leaflets of the dysplastic tricuspid valve extend toward the RV and are usually associated with tricuspid regurgitation.[79] EA is rare, with a prevalence of 5.2 per 100,000 births. It accounts for 1% of CHD but is consequential because it constitutes approximately 40% of congenital tricuspid valve malformations.[66,80] The severity of the condition depends on the extent to which the RV is filled by the enlarged right atrium, a condition known as RV atrialization.[73] There are four types, classified from A to D, based on the degree of RV atrialization. A patent foramen ovale (PFO) or ostium secundum ASD is always present.[79] As a result, pressure in the right atrium increases, leading to a right-to-left shunt.

Total anomalous pulmonary venous connection

Total anomalous pulmonary venous connection is characterized by abnormal drainage of the pulmonary veins into the systemic circulation.[81] It is a rare cardiac malformation occurring in approximately 7 per 100,000 live births.[82] Typically, the pulmonary veins drain into the left brachiocephalic vein (most common) (Figure 17), the superior or inferior vena cava, the coronary sinus, the portal vein, or, rarely, into other systemic veins. Less commonly, the pulmonary veins drain directly into the right atrium,[83] resulting in a left-to-right shunt. This condition is classified based on the location where the abnormal venous connection occurs relative to the heart. The supracardiac type accounts for 50%, the cardiac type for 20%, and the infracardiac type for 20%.[81] The mixed type is observed in 10% of cases. Physiologically, it can be characterized as obstructive or non-obstructive based on the condition of the pulmonary venous flow. Obstruction is commonly seen in the infracardiac type.[84]

Hypoplastic left heart syndrome

Hypoplastic left heart syndrome (HLHS) is a broad spectrum of anomalies characterized by hypoplasia of the left-sided structures of the heart, including the aorta, mitral valve, LV, aortic root, and ascending aorta.[85] The left atrium is typically small but may be normal or enlarged in size (Figure 18). By contrast, the right heart structures are markedly enlarged. The PFO and PDA are critical to the systemic circulation. Despite a prevalence of 1 in 5,000 live births, HLHS accounts for 7% to 9% of all CHDs diagnosed before the age of 1 year.[73] Additionally, it is the fourth most common CHD presenting in the first year of life. It may be associated with syndromes such as Noonan, Holt–Oram, Turner, or Smith–Lemli–Oplitz syndromes.[86] CT is preferred preoperatively to detect anomalies such as CoA and VSD, which may accompany HLHS. CMR is an extremely

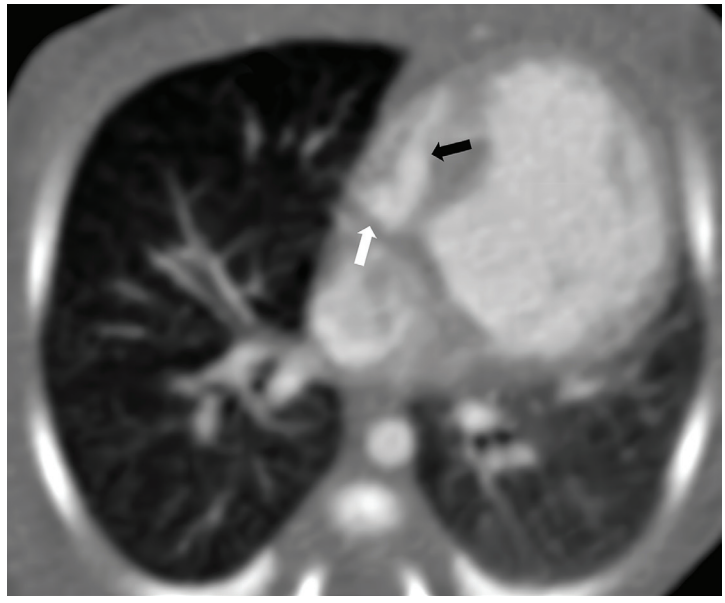

Figure 15. Tricuspid valve atresia (white arrow) and accompanying right ventricular hypoplasia (black arrow) in a 5-day-old girl with a diagnosis of tricuspid atresia.

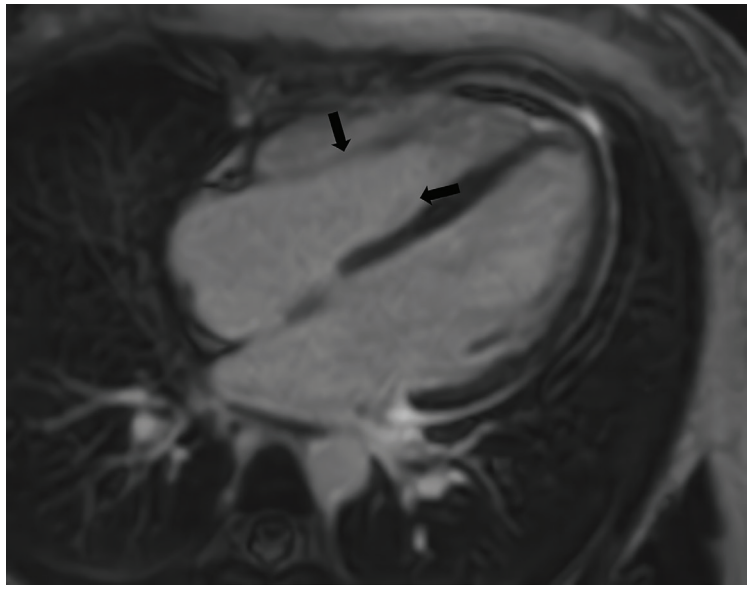

Figure 16. In the cardiac magnetic resonance examination performed on a 26-year-old female patient, a distinct extension of the tricuspid valve cusps toward the right ventricle was observed and a diagnosis of Ebstein anomaly was made (black arrows).

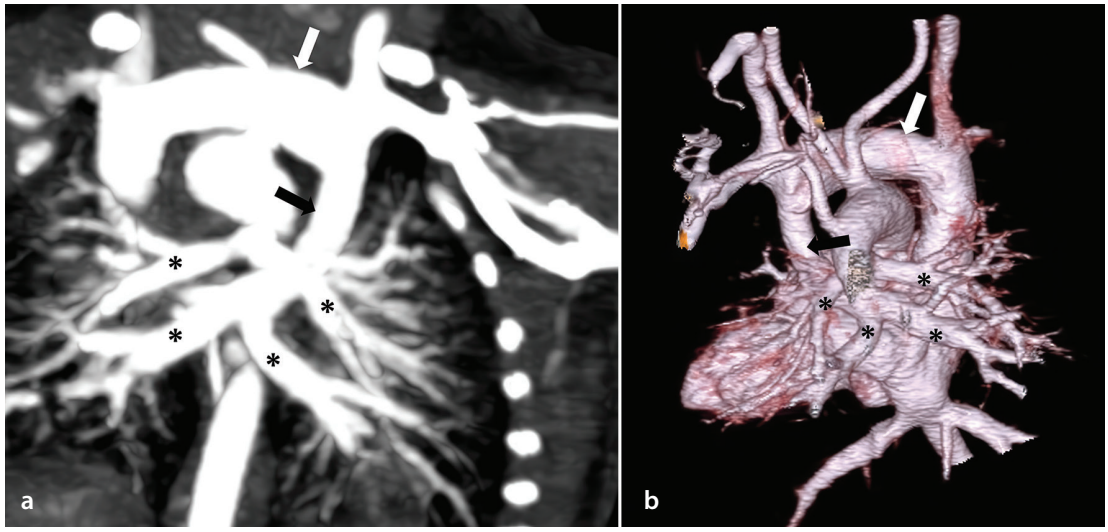

Figure 17. Coronal reformatted computed tomography angiography **(a)** and three-dimensional volume rendered image **(b)** of a 3-day-old male patient showing the pulmonary veins (black stars) opening into the left brachiocephalic vein (white arrows) via a vertical venous connection (black arrows).

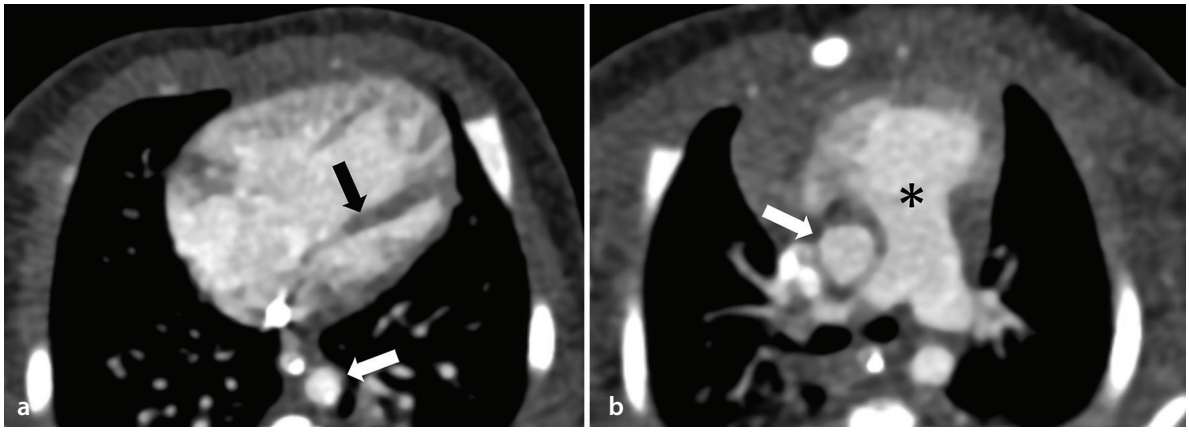

Figure 18. Axial computed tomography angiography **(a,b)** images of a 2-day-old female patient showing left ventricular hypoplasia (black arrow), aortic hypoplasia (white arrows), and accompanying pulmonary artery enlargement (black star).

important imaging modality for detecting pathologies such as endocardial fibroelastosis that may accompany HLHS, for quantitative measurement of ventricular volumes pre- and postoperatively, for functional assessment of the aortic and mitral valves, and, particularly, for detecting fibrosis, which may develop in the ventricles during postoperative follow-up.

Pulmonary atresia with intact ventricular septum

PA with intact ventricular septum (PA–IVS) is characterized by the absence of communication between the RV and LV and the presence of PA (Figure 19).[87] Moreover, the RV is hypoplastic to varying degrees. This condition is rare, occurring in 5 per 100,000 live births and accounting for 1% to 3% of CHDs.[88] Another important feature of PA–IVS is that it may be associated with other cardiac anomalies; PFO, coronary arteriovenous fistulas (10%–50%), and tricuspid insufficiency secondary to RV dilatation, as well as MAPCAs, which provide pulmonary vascularization, may be present.[88] CT is an extremely successful technique for identifying any additional pathologies, fistulas, or collateral vascular structures that may be present.[89] CMR is vital in the postoperative period for evaluating pulmonary valve and RV function and monitoring the presence of fibrosis.[90]

Single ventricle

The primary definition of single ventricle is the presence of a single ventricle into which both atria drain and the systemic and pulmonary circulation provided by this ventricle; it is a CHD (Figure 20).[91] Depending on the ventricular morphology, it is referred to as double-inlet LV, double-inlet RV, or, when differentiation is not possible, primitive ventricle.[92] The incidence of the LV type is 5–10 per 100,000 live births, making it the most common functional single ventricle defect.[93] Associated conditions include TGA (70%, typically L-type), subvalvular PS or atresia (66%), subaortic obstruction, and CoA.[72] CT and MRI are superior to echocardiography in evaluating extracardiac vascular structures, identifying associated anomalies, and assessing complex anatomical relationships. CMR has a distinct role in evaluating postoperative valve and ventricular function.[94,95]

In conclusion, CHDs represent a wide spectrum, and accurate diagnosis is vital. This is because treatment plans are specific to the patient's diagnosis. Advances in cardiac imaging in recent years have been instrumental in reducing morbidity rates and increasing life expectancy in individuals with CHD. In the evaluation of imaging methods, radiography is non-specific but can assist in determining heart size and pulmonary vas-

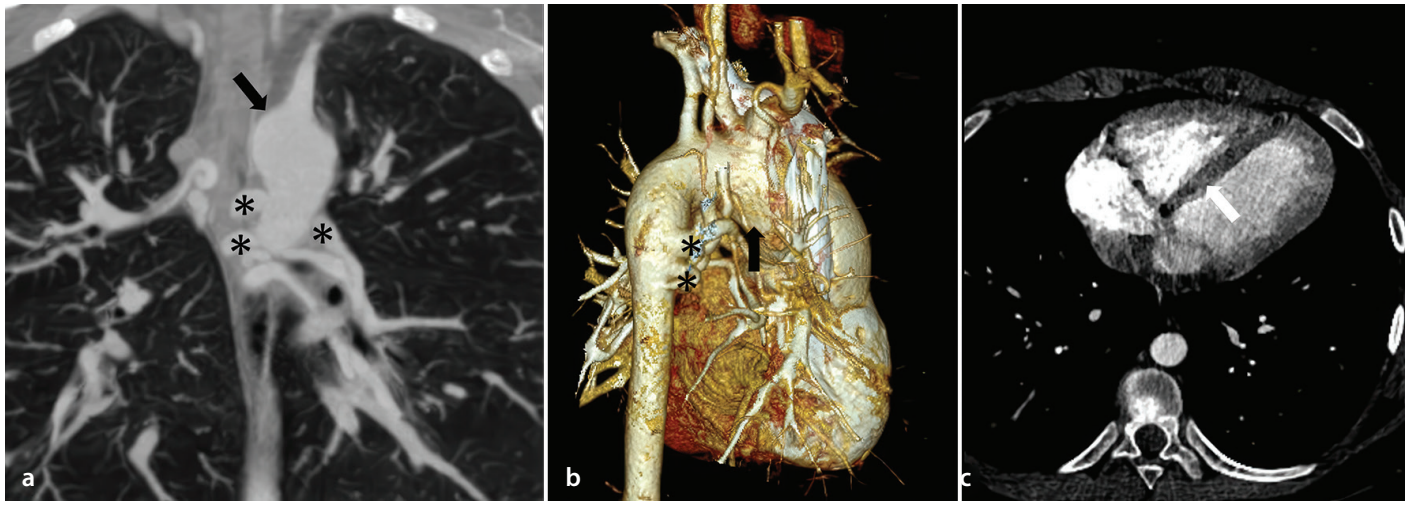

Figure 19. A 19-year-old male patient with isolated pulmonary atresia: the aorta (black arrows) is observed, but the pulmonary artery is not observed in coronal reformatted computed tomography angiography (CTA) **(a)** and three-dimensional volume rendered **(b)** images. Multiple accompanying major aortopulmonary collateral arteries are observed (black stars). In the axial CTA image **(c)**, the interventricular septum is seen intact (white arrow).

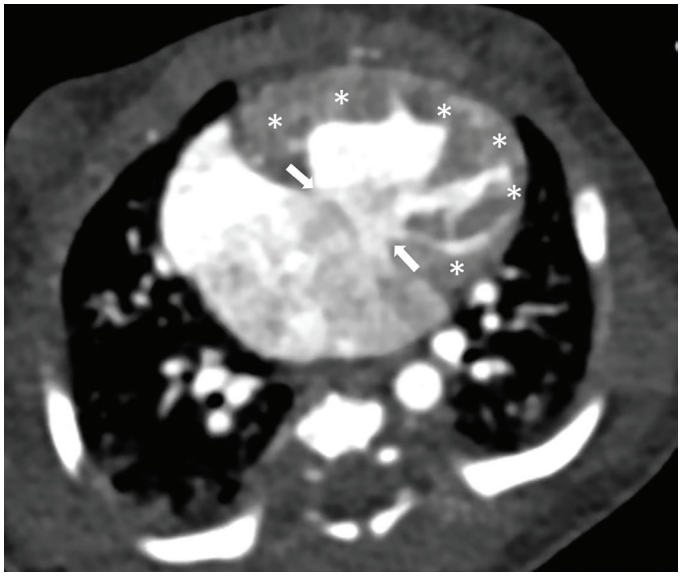

Figure 20. Axial computed tomography angiography image of a 6-day-old girl showing atrioventricular septal defect, single atrioventricular valve (white arrows), and single ventricle morphology (white stars).

cularity, whereas echocardiography is user dependent and has a limited role in evaluating extracardiac structures. Advances in imaging have led to an increasing role for CT and MRI in addition to cardiac evaluation, including the visualization of extracardiac vascular structures and postoperative follow-up. This has substantially reduced the role of invasive cardiac catheterization in the diagnosis of CHD. Ongoing technological innovations have led to non-invasive modalities with improved image quality, lower ionizing radiation and contrast doses, and reduced imaging time, thereby decreasing the need for anesthesia. Diverse modalities for detecting cyanotic CHD, along with ongoing advances in surgical procedures, will result in more patients with CHD surviving into adulthood in the future. Therefore, the role of CT and MRI will continue to expand. The appropriate selection of imaging methods is guided by the clinical context and the relative strengths of various imaging modalities. CT is preferred for the initial assessment of large vessel anatomy in newborns, especially when functional information is not important. CMR is critical for the preoperative and postoperative assessment of ventricular and valve function, measurement of flow parameters in existing shunts, and detection of myocardial fibrosis. With this approach, the proper use of imaging modalities provides the detailed anatomy and post-surgical follow-up of the patient that are important for surgical planning.

Footnotes

Conflict of Interest

The authors declared no conflicts of interest.

References

1. Stout KK, Daniels CJ, Aboulhosn JA, et al. 2018 AHA/ACC Guideline for the Management of Adults with Congenital Heart Disease: A Report of the American College of Cardiology/American Heart Association Task Force on Clinical Practice Guidelines. *J Am Coll Cardiol*. 2019;73(12):e81-e192. [Crossref]
2. Koplay M. Congenital cardiovascular anomalies: CT and MRI imaging. 1st ed. Ankara: Dünya Tıp Kitabevi; 2020.
3. Chung JH, Gunn ML, Godwin JD, Takasugi J, Kanne JP. Congenital thoracic cardiovascular anomalies presenting in adulthood: a pictorial review. *J Cardiovasc Comput Tomogr*. 20093(1 Suppl):S35-S46. [Crossref]
4. Tsai IC, Chen MC, Jan SL, et al. Neonatal cardiac multidetector row CT: why and how we do it. *Pediatr Radiol*. 2008;38(4):438-451. [Crossref]
5. Panayiotou HR, Mills LK, Broadbent DA, et al. Comprehensive neonatal cardiac, feed and wrap, non-contrast, non-sedated, free-breathing compressed sensing 4D flow mri assessment. *J Magn Reson Imaging*. 2023;57(3):789-799. [Crossref]
6. Lapierre C, Garel L, El-Jalbout R, Damphousse A, Déry J. Cardiac CT and MRI of cardiac malformations: how to interpret them? *Diagn Interv Imaging*. 2016;97(5):519-530. [Crossref]
7. Frommelt P, Lopez L, Dimas VV, et al. Recommendations for Multimodality Assessment of Congenital Coronary Anomalies: A Guide from the American Society of Echocardiography: Developed in Collaboration with the Society for Cardiovascular Angiography and Interventions, Japanese Society of

Echocardiography, and Society for Cardiovascular Magnetic Resonance. *J Am Soc Echocardiogr*. 2020;33(3):259-294. [Crossref]

8. Tricarico F, Hlavacek AM, Schoepf UJ, et al. Cardiovascular CT angiography in neonates and children: image quality and potential for radiation dose reduction with iterative image reconstruction techniques. *Eur Radiol*. 2013;23(5):1306-1315. [Crossref]
9. Siripornpitak S, Pornkul R, Khowsathit P, Layangool T, Promphan W, Pongpanich B. Cardiac CT angiography in children with congenital heart disease. *Eur J Radiol*. 2013;82(7):1067-1082. [Crossref]
10. Bailliard F, Hughes ML, Taylor AM. Introduction to cardiac imaging in infants and children: techniques, potential, and role in the imaging work-up of various cardiac malformations and other pediatric heart conditions. *Eur J Radiol*. 2008;68(2):191-198. [Crossref]
11. Hellinger JC, Pena A, Poon M, Chan FP, Epelman M. Pediatric computed tomographic angiography: imaging the cardiovascular system gently. *Radiol Clin North Am*. 2010r;48(2):439-467. [Crossref]
12. Schicchi N, Fogante M, Esposto Pirani P, et al. Third-generation dual-source dual-energy CT in pediatric congenital heart disease patients: state-of-the-art. *Radiol Med*. 2019;124(12):1238-1252. [Crossref]
13. Krishnamurthy R. Neonatal cardiac imaging. *Pediatr Radiol*. 2010;40(4):518-527. [Crossref]
14. Kravchenko D, Hart C, Garbe S, et al. Image quality and radiation dose of dual source high pitch computed tomography in pediatric congenital heart disease. *Sci Rep*. 2022;12(1):9934. [Crossref]
15. Sun Z. Multislice CT angiography in cardiac imaging: prospective ECG-gating or retrospective ECG-gating? *Biomed Imaging Interv J*. 2010;6(1):e4. [Crossref]
16. Dirrichs T, Tietz E, Rüffer A, et al. Photon-counting versus dual-source CT of congenital heart defects in neonates and infants: initial experience. *Radiology*. 2023;307(5):e223088. [Crossref]
17. Dillman JR, Hernandez RJ. Role of CT in the evaluation of congenital cardiovascular disease in children. *AJR Am J Roentgenol*. 2009;192(5):1219-1231. [Crossref]
18. Stolzmann P, Leschka S, Scheffel H, et al. Dual-source CT in step-and-shoot mode: non-invasive coronary angiography with low radiation dose. *Radiology*. 2008;249(1):71-80. [Crossref]
19. Paul JF, Abada HT. Strategies for reduction of radiation dose in cardiac multislice CT. *Eur Radiol*. 2007;17(8):2028-2037. [Crossref]
20. Han BK, Rigsby CK, Hlavacek A, et al. Computed tomography imaging in patients with congenital heart disease part I: rationale and utility. an expert consensus document of the society of cardiovascular computed tomography (SCCT): endorsed by the Society of Pediatric Radiology (SPR) and the North American Society of Cardiac Imaging (NASCI). *J Cardiovasc Comput Tomogr*. 2015;9(6):475-492. [Crossref]
21. Zamorano JL, Bax J, Lancellotti P, Knuuti J, Badano L. The ESC Textbook of Cardiovascular Imaging: Oxford University Press, USA; 2015. [Crossref]
22. Kilner PJ, Geva T, Kaemmerer H, Trindade PT, Schwitter J, Webb GD. Recommendations for cardiovascular magnetic resonance in adults with congenital heart disease from the Respective Working Groups of the European Society of Cardiology. *Eur Heart J*. 2010;31(7):794-805. [Crossref]
23. Biglands JD, Radjenovic A, Ridgway JP. Cardiovascular magnetic resonance physics for clinicians: part II. *J Cardiovasc Magn Reson*. 2012;14(1):66. [Crossref]
24. Ridgway JP. Cardiovascular magnetic resonance physics for clinicians: part I. *J Cardiovasc Magn Reson*. 2010;12(1):71. [Crossref]
25. Vahanian A, Alfieri O, Andreotti F, et al. Guidelines on the management of valvular heart disease (version 2012): the Joint Task Force on the Management of Valvular Heart Disease of the European Society of Cardiology (ESC) and the European Association for Cardio-Thoracic Surgery (EACTS). *Eur J Cardiothorac Surg*. 2012;42(4):1-44. [Crossref]
26. Di Salvo G, Miller O, Babu Narayan S, et al. Imaging the adult with congenital heart disease: a multimodality imaging approach-position paper from the eacvi. *Eur Heart J Cardiovasc Imaging*. 2018;19(10):1077-1098. [Crossref]
27. Lee GH, Koo HJ, Park KJ, Yang DH, Ha H. Characterization of baseline hemodynamics after the Fontan procedure: a retrospective cohort study on the comparison of 4D flow MRI and computational fluid dynamics. *Front Physiol*. 2023;14:1199771. [Crossref]
28. Pednekar AS, Wang H, Flamm S, Cheong BY, Muthupillai R. Two-center clinical validation and quantitative assessment of respiratory triggered retrospectively cardiac gated balanced-ssfp cine cardiovascular magnetic resonance imaging in adults. *J Cardiovasc Magn Reson*. 2018;20(1):44. [Crossref]
29. Taylor AM, Dymarkowski S, Hamaekers P, et al. MR coronary angiography and late-enhancement myocardial MR in children who underwent arterial switch surgery for transposition of great arteries. *Radiology*. 2005;234(2):542-547. [Crossref]
30. Bonnichsen C, Ammash N. Choosing between MRI and CT imaging in the adult with congenital heart disease. *Curr Cardiol Rep*. 2016;18(5):45. [Crossref]
31. Dorfman AL, Geva T, Samyn MM, et al. SCMR expert consensus statement for cardiovascular magnetic resonance of acquired and non-structural pediatric heart disease. *J Cardiovasc Magn Reson*. 2022;24(1):44. [Crossref]
32. Schulz-Menger J, Bluemke DA, Bremerich J, et al. Standardized image interpretation and post-processing in cardiovascular magnetic resonance - 2020 update : Society for Cardiovascular Magnetic Resonance (SCMR): Board of Trustees Task Force on Standardized Post-Processing. *J Cardiovasc Magn Reson*. 2020;22(1):19. [Crossref]
33. Hoffman JI, Kaplan S. The incidence of congenital heart disease. *J Am Coll Cardiol*. 2002;39(12):1890-1900. [Crossref]
34. Puranik R, Muthurangu V, Celermajer DS, Taylor AM. Congenital heart disease and multi-modality imaging. *Heart Lung Circ*. 2010;19(3):133-144. [Crossref]
35. Wald RM, Powell AJ. Simple congenital heart lesions. *J Cardiovasc Magn Reson*. 2006;8(4):619-631. [Crossref]
36. Khanna A, Litt HI. ECG-gated MDCT of left-to-right shunt flow through a ventricular septal defect. *AJR Am J Roentgenol*. 2004;183(6):1838. [Crossref]
37. Ropers D, Regenfus M, Wasmeier G, et al. [Ventricular septum defect: imaging using computer tomography, magnetic resonance tomography and color doppler echocardiography]. *Dtsch Med Wochenschr*. 2007;132(14):769-770. [Crossref]
38. Backer CL, Stewart RD, Mavroudis C. Overview: history, anatomy, timing, and results of complete atrioventricular canal. *Semin Thorac Cardiovasc Surg Pediatr Card Surg Annu*. 2007:3-10. [Crossref]
39. Allen HD, Driscoll DJ, Shaddy RE, Feltes TF, editors. Moss & Adams' heart disease in infants, children, and adolescents: including the fetus and young adult. 8th ed. Philadelphia: Lippincott Williams & Wilkins; 2013.
40. Park MK. Pediatric cardiology for practitioners. 5th ed. Part 2: Special tools in evaluation of cardiac patients. Chapter 6: Noninvasive techniques. Philadelphia: Mosby Elsevier; 2008.
41. Saremi F, Hassani C, Sánchez-Quintana D. Septal atrioventricular junction region: comprehensive imaging in adults. *Radiographics*. 2016;36(7):1966-1986. [Crossref]
42. Prsa M, Sun L, van Amerom J, et al. Reference ranges of blood flow in the major vessels of the normal human fetal circulation at term by phase-contrast magnetic resonance imaging. *Circ Cardiovasc Imaging*. 2014;7(4):663-670. [Crossref]
43. Körperich H, Gieseke J, Barth P, et al. Flow volume and shunt quantification in pediatric congenital heart disease by real-time magnetic resonance velocity mapping: a validation study. *Circulation*. 2004;109(16):1987-1993. [Crossref]
44. Moore P, Brook M. Patent Ductus Arteriosus and Aorticopulmonary Window. In: Allen Hd,

Driscoll Dj, Shaddy Re, Feltes Tf, eds. Moss and Adams' Heart Disease. *Wolters Philadelphia, ABD: Kluwer-Lipincott Williams& Wilkins;* 2013;8:722-745. [Crossref]

45. Takahashi Y, Roman C, Chemtob S, et al. Cyclooxygenase-2 inhibitors constrict the fetal lamb ductus arteriosus both *in vitro* and *in vivo*. *Am J Physiol Regul Integr Comp Physiol*. 2000;278(6):R1496-R1505. [Crossref]
46. Burkett DA. Common left-to-right shunts. *Pediatr Clin North Am*. 2020;67(5):821-842. [Crossref]
47. Krichenko A, Benson LN, Burrows P, Möes CA, McLaughlin P, Freedom RM. Angiographic classification of the isolated, persistently patent ductus arteriosus and implications for percutaneous catheter occlusion. *Am J Cardiol*. 1989;63(12):877-880. [Crossref]
48. Schena F, Francescato G, Cappelleri A, et al. Association between hemodynamically significant patent ductus arteriosus and bronchopulmonary dysplasia. *J Pediatr*. 2015;166(6):1488-1492. [Crossref]
49. Kato R, Lickfett L, Meininger G, et al. Pulmonary vein anatomy in patients undergoing catheter ablation of atrial fibrillation: lessons learned by use of magnetic resonance imaging. *Circulation*. 2003;107(15):2004-2010. [Crossref]
50. Alsoufi B, Cai S, Van Arsdell GS, Williams WG, Caldarone CA, Coles JG. Outcomes after surgical treatment of children with partial anomalous pulmonary venous connection. *Ann Thorac Surg*. 2007;84(6):2020-2026. [Crossref]
51. Furlanetto G, Furlanetto BH, Henriques SR, et al. Mixed type total anomalous pulmonary venous connection: early results and surgical techniques. *World J Pediatr Congenit Heart Surg*. 2015;6(1):26-32. [Crossref]
52. Liu CW, Hwang B, Lee BC, Lu JH, Meng LC. Aortic stenosis in children: 19-year experience. *Zhonghua Yi Xue Za Zhi (Taipei)*. 1997;59(2):107-113. [Crossref]
53. Lancellotti P, Zamorano JL, Habib G, Badano L. The EACVI Textbook of Echocardiography: Oxford University Press; 2016. [Crossref]
54. Marchini F, Meossi S, Passarini G, Campo G, Pavasini R. Pulmonary valve stenosis: from diagnosis to current management techniques and future prospects. *Vasc Health Risk Manag*. 2023;19:379-390. [Crossref]
55. Singh S, Hakim FA, Sharma A, et al. Hypoplasia, pseudocoarctation and coarctation of the aorta - a systematic review. *Heart Lung Circ*. 2015;24(2):110-118. [Crossref]
56. Karaosmanoglu AD, Khawaja RD, Onur MR, Kalra MK. CT and MRI of aortic coarctation: pre- and postsurgical findings. *AJR Am J Roentgenol*. 2015;204(3):W224-W233. [Crossref]
57. Nie P, Wang X, Cheng Z, et al. The value of low-dose prospective ECG-gated dual-source CT angiography in the diagnosis of coarctation of the aorta in infants and children. *Clin Radiol*. 2012;67(8):738-745. [Crossref]
58. Hughes D Jr, Siegel MJ. Computed tomography of adult congenital heart disease. *Radiol Clin North Am*. 2010;48(4):817-835. [Crossref]
59. Kim HK, Gottliebson W, Hor K, et al. Cardiovascular anomalies in Turner syndrome: spectrum, prevalence, and cardiac MRI findings in a pediatric and young adult population. *AJR Am J Roentgenol*. 2011;196(2):454-460. [Crossref]
60. Hanneman K, Newman B, Chan F. Congenital variants and anomalies of the aortic arch. *Radiographics*. 2017;37(1):32-51. [Crossref]
61. Gruber PJ, Epstein JA. Development gone awry: congenital heart disease. *Circ Res*. 2004;94(3):273-283. [Crossref]
62. Mulay AV, Watterson KG. Isolated Right Subclavian Artery, Interrupted Aortic Arch, and Ventricular Septal Defect. *Ann Thorac Surg*. 1997;63(4):1163-1165. [Crossref]
63. Apitz C, Webb GD, Redington AN. Tetralogy of fallot. *Lancet*. 2009;374(9699):1462-1471. [Crossref]
64. Syed MA, Mohiaddin RH. Magnetic resonance imaging of congenital heart disease: Springer Nature; 2023. [Crossref]
65. Moscatelli S, Pergola V, Motta R, et al. Multimodality imaging assessment of tetralogy of fallot: from diagnosis to long-term follow-up. *Children (Basel)*. 2023;10(11):1747. [Crossref]
66. Warmerdam EG, Neijzen RL, Voskuil M, Leiner T, Grotenhuis HB. Four-dimensional flow CMR in tetralogy of fallot: current perspectives. *Br J Radiol*. 2022;95(1133):20210298. [Crossref]
67. Cohen MS, Eidem BW, Cetta F, et al. Multimodality ımaging guidelines of patients with transposition of the great arteries: a report from the American Society of Echocardiography Developed in Collaboration with the Society for Cardiovascular Magnetic Resonance and the Society of Cardiovascular Computed Tomography. *J Am Soc Echocardiogr*. 2016;29(7):571-621. [Crossref]
68. Canan A, Ashwath R, Agarwal PP, François C, Rajiah P. Multimodality imaging of transposition of the great arteries. *Radiographics*. 2021;41(2):338-360. [Crossref]
69. Chan FP, Hanneman K. Computed tomography and magnetic resonance imaging in neonates with congenital cardiovascular disease. *Semin Ultrasound CT MR*. 2015;36(2):146-160. [Crossref]
70. Syamasundar Rao P. Diagnosis and management of cyanotic congenital heart disease: part II. *Indian J Pediatr*. 2009;76(3):297-308. [Crossref]
71. Goo HW. Cardiac MDCT in children: CT technology overview and interpretation. *Radiol Clin North Am*. 2011;49(5):997-1010. [Crossref]
72. Rao PS. Diagnosis and management of cyanotic congenital heart disease: part I. *Indian J Pediatr*. 2009;76(1):57-70. [Crossref]
73. Rao PS. Consensus on timing of intervention for common congenital heart diseases: part II - cyanotic heart defects. *Indian J Pediatr*. 2013;80(8):663-674. [Crossref]
74. Koplay M, Cimen D, Sivri M, et al. Truncus arteriosus: diagnosis with dual-source computed tomography angiography and low radiation dose. *World J Radiol*. 2014;6(11):886-889. [Crossref]
75. Singh AAV, Yoo SJ, Seed M, Lam CZ, Valverde I. Recent advances in multimodal imaging in tetralogy of fallot and double outlet right ventricle. *Curr Opin Cardiol*. 2024;39(4):323-330. [Crossref]
76. Frank L, Dillman JR, Parish V, et al. Cardiovascular MR imaging of conotruncal anomalies. *Radiographics*. 2010;30(4):1069-1094. [Crossref]
77. Dewi DK, Perdhana DP. Double outlet right ventricle presenting in an adult woman: a case report. *Radiol Case Rep*. 2022;17(5):1413-1415. [Crossref]
78. Zucker EJ, Koning JL, Lee EY. Cyanotic congenital heart disease: essential primer for the practicing radiologist. *Radiol Clin North Am*. 2017;55(4):693-716. [Crossref]
79. Malik SB, Kwan D, Shah AB, Hsu JY. The right atrium: gateway to the heart--anatomic and pathologic imaging findings. *Radiographics*. 2015;35(1):14-31. [Crossref]
80. Negoi RI, Ispas AT, Ghiorghiu I, et al. Complex Ebstein's malformation: defining preoperative cardiac anatomy and function. *J Card Surg*. 2013;28(1):70-81. [Crossref]
81. Files MD, Morray B. Total anomalous pulmonary venous connection: preoperative anatomy, physiology, ımaging, and ınterventional management of postoperative pulmonary venous obstruction. *Semin Cardiothorac Vasc Anesth*. 2017;21(2):123-131. [Crossref]
82. Seale AN, Uemura H, Webber SA, et al. Total anomalous pulmonary venous connection: morphology and outcome from an international population-based study. *Circulation*. 2010;122(25):2718-2726. [Crossref]
83. Gaca AM, Jaggers JJ, Dudley LT, Bisset GS, 3rd. Repair of congenital heart disease: a primer--part 2. *Radiology*. 2008;248(1):44-60. [Crossref]
84. Karamlou T, Gurofsky R, Al Sukhni E, et al. Factors associated with mortality and reoperation in 377 children with total anomalous pulmonary venous connection. *Circulation*. 2007;115(12):1591-1598. [Crossref]
85. Pedra SRFF. Imaging for hypoplastic left heart syndrome. *World J Pediatr Congenit Heart Surg*. 2022;13(5):571-575. [Crossref]
86. Connor JA, Thiagarajan R. Hypoplastic left heart syndrome. *Orphanet J Rare Dis*. 2007;2:23. [Crossref]
87. Chikkabyrappa SM, Loomba RS, Tretter JT. Pulmonary Atresia with an intact ventricular

septum: preoperative physiology, imaging, and management. *Semin Cardiothorac Vasc Anesth*. 2018;22(3):245-255. [Crossref]

88. Uribe S, Bächler P, Valverde I, et al. Hemodynamic assessment in patients with one-and-a-half ventricle repair revealed by four-dimensional flow magnetic resonance imaging. *Pediatr Cardiol*. 2013;34(2):447-451. [Crossref]
89. Hascoet S, Combelles S, Acar P. Cardiac computed tomography of multiple coronary arteries to right ventricle fistulas in a newborn with pulmonary atresia and intact ventricular septum. *Can J Cardiol*. 2014;30(2):247. [Crossref]
90. Liang XC, Lam WW, Cheung EW, Wu AK, Wong SJ, Cheung YF. Restrictive right ventricular physiology and right ventricular fibrosis as assessed by cardiac magnetic resonance and exercise capacity after biventricular repair of pulmonary atresia and intact ventricular septum. *Clin Cardiol*. 2010;33(2):104-110. [Crossref]
91. Wilkinson JL, Anderson RH. Anatomy of functionally single ventricle. *World J Pediatr Congenit Heart Surg*. 2012;3(2):159-164. [Crossref]
92. Festa P, Ait Ali L, Bernabei M, De Marchi D. The role of magnetic resonance imaging in the evaluation of the functionally single ventricle before and after conversion to the Fontan circulation. *Cardiol Young*. 2005;15(Suppl 3):51-56. [Crossref]
93. Güvenç O, Saygi M, Şengül FS, Ayyıldız P, Güzeltaş A. Double inlet left ventricle-ventriculoarterial discordance without surgical treatment. *Pediatr Int*. 2016;58(6):509-511. [Crossref]
94. Ito D, Shiraishi J, Noritake K, Kohno Y. Multidetector computed tomography demonstrates double-inlet, double-outlet right ventricle. *Intern Med*. 2011;50(18):2053-2054. [Crossref]
95. Rathod RH, Prakash A, Kim YY, et al. Cardiac magnetic resonance parameters predict transplantation-free survival in patients with fontan circulation. *Circ Cardiovasc Imaging*. 2014;7(3):502-509. [Crossref]